IEEE Access
Multidisciplinary | Rapid Review | Open Access Journal

Received November 9, 2021, accepted December 10, 2021, date of publication December 22, 2021,
date of current version December 31, 2021.

Digital Object Identifier 10.1109/ACCESS.2021.3137480

Simple Design on Nanoscale Receivers Using CNT Cantilevers

YUJI ITO, (Member, IEEE), AND YUKIHIRO TADOKORO, (Senior Member, IEEE)
Toyota Central R&D Labs., Inc., Nagakute-shi, Aichi 480-1192, Japan
Corresponding author: Yuji Ito (ito-yuji@mosk.tytlabs.co.jp)

ABSTRACT To develop nanoscale sensors with future potential, a nanoscale receiver utilizing the nanomechanical vibration of a cantilever composed of a carbon nanotube, had been proposed for detecting the digital information carried by wireless signals. The introduced receiver includes two essential parts: a phase detector and demodulator, which employ a reference signal and carrier signal, respectively. Additional components such as electrical circuits and oscillators are required to excite these signals, increasing the sensor size. This study presents a design method for simplifying the receiver structure to contribute to sensor miniaturization. This study theoretically derives a tractable form that can describe the performance of the introduced receiver. This form enables the determination of a simple receiver structure with performance enhancement from a mathematical perspective. Using the proposed method, either the reference wave or carrier signal can be excluded from the receiver, simplifying its structure. The results are demonstrated through a numerical simulation.

INDEX TERMS Carbon nanotubes, differential equations, nanoelectromechanical systems, phase detection.

I. INTRODUCTION

Nanomechanical devices including physical, chemical, and biological sensors have the potential to realize next-generation sensing systems [1]–[9]. Wireless networks using nanoscale sensors, called the Internet of Nano-Things, provide a promising new communication paradigm [10]–[12]. For such nanoscale networks, the routing protocols [13], [14], transmission policies [15], and localization methods [16] have been discussed. Many applications have been envisioned using nanoscale networks in the biomedical field, including health monitoring and therapy [17]–[19]. Other prospective applications include invisible imaging via numerous nanoscale sensors [20], [21]. Moreover, big data analytics combined with nanoscale networks has been focused upon [22]. To establish such networks, communication between nanoscale sensors is essential for transmitting and aggregating the measured quantities. However, conventional electromagnetic-based antennas cannot be applied in nanoscale networks, because the antenna size is of the order of the transmitted signal wavelength [23]; for example, the size of an antenna in the megahertz band is several centimeters. Although using signals in the terahertz band may downsize the antennas [24]–[26], additional cost is incurred in developing circuits and systems.

To address this problem, several types of miniaturized antennas have been discussed [17], [27]–[32]. One promising technique involves a nanomechanical resonator, in which physical quantities can be measured by observing the mechanical vibration in the resonant mode [33], [34]. One typical example is carbon nanotube (CNT) cantilevers; the behavior of nanomechanical vibration is traditionally described using the Duffing equation [2], [7], [35], [36]. Recently, by focusing on CNT nanocantilevers or a nanobeam, a detailed model with strain- and stress-driven nonlocal mechanics has been developed [37]–[39]. Such a nanocantilever is capable of detecting electromagnetic waves [27]–[29]. In particular, the nanoscale receiver theoretically presented in [29] can detect the phase of an incoming electromagnetic wave. As the phase describes the transmitted digital data, this detection enables data transfer; however, an additional reference electromagnetic wave and carrier signal are required for the detection, complicating the receiver structure. The receiver should be equipped with additional devices to generate such a wave and signal. Thereby, the advantage of the receiver being infinitesimal is still missing. The detection of digitally modulated signals with a nonlinear vibration mode has been theoretically addressed [40];

The associate editor coordinating the review of this manuscript and approving it for publication was Jenny Mahoney.

however, it needs careful design of the nonlinear parameters and signal amplitude.

To overcome this problem, we propose a design method that simplifies the receiver structure proposed in [29]. A performance index for the phase detection is formulated as a function of the CNT motion. This performance index is transformed into a tractable form through a decomposition method. By analyzing the tractable form, we provide two types of simplified receivers that omit either the carrier signal or reference wave. The main contributions of this study are summarized as follows.

- We derive a theoretical design method to simplify the receiver structure, as shown in Theorems 1 and 2. These theorems provide appropriate design parameters for excluding either the carrier signal or reference wave from the receiver, simplifying the receiver structure.
- We perform a numerical simulation to show the effectiveness of the proposed design method and evaluate the two types of simplified receivers designed according to Theorems 1 and 2, respectively. Further, we numerically show that both the receivers perform successfully.

Through both theoretical and numerical approaches, we demonstrate that the receiver structure is successfully simplified. The results of this study have been applied in our relevant work that focuses on the control of nanomechanical systems [41]. Instead of the CNT, vertically grown silicon nanowires or high aspect ratio silicon structures could be used.

The remainder of this paper is organized as follows. Section II introduces the configuration of the nanoscale receiver proposed in [29] and reviews its mathematical models. The main problem in simplifying the receiver structure is described in Section III. Section IV proposes a design method to address this problem. A numerical example is presented in Section V to demonstrate the proposed method. Section VI summarizes the paper and mentions the scope for future research.

II. SYSTEM CONFIGURATION

This section reviews the configuration of the nanoscale receiver proposed in [29]. The receiver includes a phase detector and demodulator, as shown in Fig. 1. It obtains information on the phase $\theta_{\rm in}$ of the incoming wave $E_{\rm in}(t)$ sent from the transmitter. In the phase detector, the CNT is arrayed on the cathode, which is connected to ground. Applying the voltage V to the anode excites a charge around the tip of the CNT. This tip is subjected to an electric force generated by the charge, incoming wave $E_{\rm in}(t)$, and reference wave $E_{\rm r}(t)$ according to Coulomb's law. The electric force is sinusoidal because the incoming wave $E_{\rm in}(t)$ is a cosine wave with the offset phase $\theta_{\rm in}$. The sinusoidal force vibrates the tip, depending on the phase $\theta_{\rm in}$. Meanwhile, a field emission current generated by the voltage V flows from the CNT tip to the anode. The time series of this current depends on the vibration of the tip, i.e., the phase $\theta_{\rm in}$. The demodulator extracts the

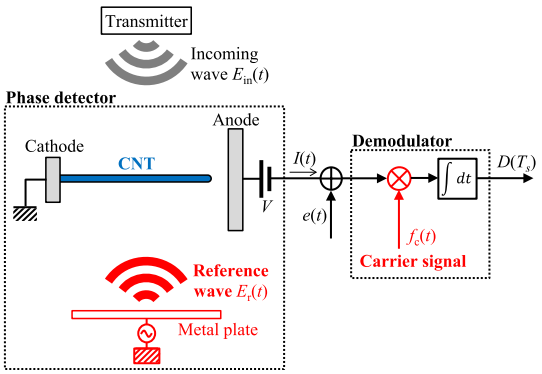

(a) Overall structure of the receiver

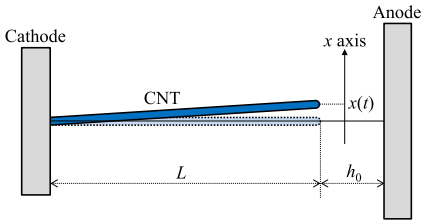

(b) Detailed configuration of the CNT cantilever

FIGURE 1. Configuration of the nanoscale receiver proposed in [29]. In the proposed design method, either the reference wave or carrier signal can be omitted.

binary information associated with the phase $\theta_{\rm in}$ from the current, under an appropriate setting of the carrier signal. The mathematical models used in the nanoscale receiver are introduced in the following subsections.

A. INCOMING WAVE

The incoming wave sent from the transmitter [29] is defined as

$$E_{\rm in}(t) := A_{\rm in}\cos(\omega_{\rm in}t + \theta_{\rm in}), \tag{1}$$

where $t \geq 0$, $A_{\rm in} > 0$, $\omega_{\rm in} > 0$, and $\theta_{\rm in} \in \{\theta_{\rm in}^+, \theta_{\rm in}^-\}$ are the time, amplitude, angular frequency, and phase, respectively. The phases $\theta_{\rm in}^+$ and $\theta_{\rm in}^-$ are arbitrarily designed corresponding to the one-bit information $\{+, -\}$, respectively. The receiver attempts to distinguish the two phases. The superscripts $(\cdot)^+$ and $(\cdot)^-$ used in the manuscript denote the variables/functions corresponding to $\theta_{\rm in}^+$ and $\theta_{\rm in}^-$, respectively.

B. PHASE DETECTOR

The phase detector converts the motion of the CNT tip into a field emission current [29]. Assuming that the displacement $x(t)$ of the CNT tip is sufficiently small, the motion equation with respect to $x(t)$ is modeled as a linear differential equation:

$$m\frac{{\rm d}^2x(t)}{{\rm d}t^2} + \gamma\frac{{\rm d}x(t)}{{\rm d}t} + kx(t) = q(E_{\rm in}(t) - E_{\rm r}(t)), \tag{2}$$

where $q > 0$, $m > 0$, $\gamma > 0$, and $k > 0$ are the amount of the charge around the tip, effective mass, viscosity, and elasticity, respectively. The field emission current $I(t)$ generated along with the motion of $x(t)$ is approximated as

a quadratic function of $x(t)$:

$$I(t) \approx I_0 + I_1 x(t)^2, \tag{3}$$

where I_0 and I_1 are constants. Approximating $I(t)$ as a higher-order function may improve the modeling accuracy of $I(t)$ when the displacement $x(t)$ of the CNT tip is significantly large and thus obeys a nonlinear oscillation. However, this study addresses the case where $x(t)$ is sufficiently small compared with the CNT length. The approximation with the quadratic function in (3) is reasonable in this case because the high-order terms of small $x(t)$ are negligible.

C. DEMODULATOR

The demodulator extracts the phase information from the field emission current [29]. Let T_s be the symbol duration over which the field emission current $I(t)$ is integrated:

$$T_s := \frac{2\pi}{\omega_{\rm in}} s, \tag{4}$$

where $s \in \mathbb{N}$ denotes the number of periods. The demodulator combines the field emission current $I(t)$ with the carrier signal $f_{\rm c}(t)$ and integrates it with the noise $e(t)$:

$$\begin{aligned} D(T_s) &:= \frac{1}{T_s}\int_0^{T_s} (I(t) + e(t)) f_{\rm c}(t) {\rm d}t \\ &= D_0(T_s) + n_e(T_s), \end{aligned} \tag{5}$$

where $D_0(T_s) := D(T_s)|_{e(t)=0}$. The output signal $D(T_s)$ determines the estimate of $\theta_{\rm in}$ between $\theta_{\rm in}^+$ and $\theta_{\rm in}^-$, under the assumption that it can be determined whether $D_0^+(T_s) < D_0^-(T_s)$ or $D_0^+(T_s) > D_0^-(T_s)$.

To evaluate the phase detection accuracy, the performance index expresses the difference between the output signals corresponding to the phases $\theta_{\rm in}^+$ and $\theta_{\rm in}^-$. Hence, we define the following performance index in this study:

$$\begin{aligned} J(T_s) &:= \left| \frac{I_1}{T_s}\int_0^{T_s} (x^+(t)^2 - x^-(t)^2) f_{\rm c}(t) {\rm d}t \right| \\ &\approx |D_0^+(T_s) - D_0^-(T_s)|, \end{aligned} \tag{6}$$

where the above relation is derived from (3) and (5).

III. PROBLEM SETTING

The objective of this study is to simplify the receiver structure with enhancing its phase detection performance. Accordingly, we design the reference wave $E_{\rm r}(t)$, carrier signal $f_{\rm c}(t)$, phase $\theta_{\rm in}^+$, and $\theta_{\rm in}^-$. The performance enhancement corresponds to maximizing the index $J(T_s)$ in (6). The main design problem addressed in this study is as follows:

Main design problem: *Design $E_{\rm r}(t)$, $f_{\rm c}(t)$, $\theta_{\rm in}^+$, and $\theta_{\rm in}^-$ such that the receiver structure is simplified and the performance index $J(T_s)$ is maximized.*

The next section presents two solutions to the main design problem: a receiver without a carrier signal and a receiver without a reference wave, as illustrated in Figs. 2 (a) and (b), respectively. The performance index $J(T_s)$ is approximately maximized with respect to certain design parameters.

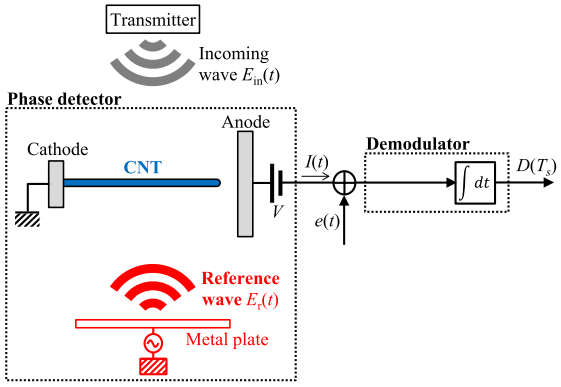

(a) Without a carrier signal using Theorem 1

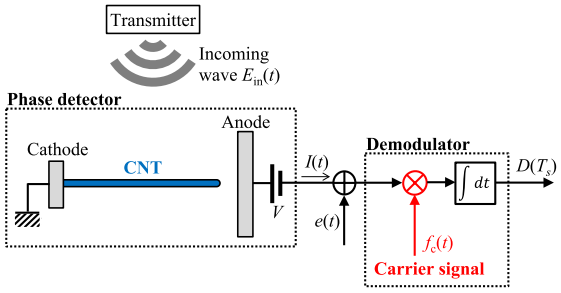

(b) Without a reference wave using Theorem 2

FIGURE 2. Simple receiver design using the proposed method.

IV. PROPOSED DESIGN METHOD

This section provides solutions to the main problem, i.e., the design of $E_{\rm r}(t)$, $f_{\rm c}(t)$, $\theta_{\rm in}^+$, and $\theta_{\rm in}^-$. We derive two theorems to design these functions and parameters, as given below. Theorem 1 states that a receiver without a carrier signal, as depicted in Fig. 2 (a), can be realized and its performance can be enhanced. Theorem 2 suggests a case without a reference wave, as depicted in Fig. 2 (b).

A difficulty involved in the main design problem is that the performance index $J(T_s)$ in (6) is not expressed as an explicit function of $E_{\rm r}(t)$, $f_{\rm c}(t)$, $\theta_{\rm in}^+$, and $\theta_{\rm in}^-$. To address this difficulty, we approximate the index $J(T_s)$ as an explicit function $\overline{J}(E_{\rm r}, f_{\rm c}, \theta_{\rm in}^+, \theta_{\rm in}^-)$ by replacing the displacement $x(t)$ in $J(T_s)$ with its steady-state solution $\overline{x}(t)$ as follows:

$$J(T_s) \approx \overline{J}(E_{\rm r}, f_{\rm c}, \theta_{\rm in}^+, \theta_{\rm in}^-), \tag{7}$$

$$\overline{J}(E_{\rm r}, f_{\rm c}, \theta_{\rm in}^+, \theta_{\rm in}^-) := \left| \frac{I_1}{T_1}\int_0^{T_1} (\overline{x}^+(t)^2 - \overline{x}^-(t)^2) f_{\rm c}(t) {\rm d}t \right|, \tag{8}$$

where $\overline{x}^+(t)$ and $\overline{x}^-(t)$ are the steady-state solutions to the motion equation (2) corresponding to $\theta_{\rm in}^+$ and $\theta_{\rm in}^-$, respectively. Considering a sufficiently large symbol duration T_s, $x(t)$ is close to $\overline{x}(t)$, which justifies the approximation. This approximation has been exploited in our relevant work; the details are provided in [41, Appendix].

The key point of this study is to analyze the approximate index $\overline{J}(E_{\rm r}, f_{\rm c}, \theta_{\rm in}^+, \theta_{\rm in}^-)$ for solving the main design problem. In Section IV-A, we focus on the decomposition of the steady-state solutions. The decomposition method transforms the performance index into a tractable form for the design. Using this tractable index, Section IV-B derives two main results to

design $E_r(t)$, $f_c(t)$, θ_{in}^+, and θ_{in}^- for simplification and performance improvement.

A. ANALYSIS OF THE PERFORMANCE INDEX

This subsection presents a technique to transform the index $\overline{J}(E_r, f_c, \theta_{in}^+, \theta_{in}^-)$ in (8) into a tractable form. The following definition is used.

Definition 1: For a given wave $E(t) := A\cos(\omega_{in}t + \theta)$ *with any* $\omega_{in} > 0$, $A \in \mathbb{R}$, *and* $\theta_\ell \in \mathbb{R}$, $\overline{x}_E(t)$ *denotes a periodic solution to the following motion equation*:

$$m\frac{d^2\tilde{x}(t)}{dt^2} + \gamma\frac{d\tilde{x}(t)}{dt} + k\tilde{x}(t) = qE(t), \tag{9}$$

where $\overline{x}_E(t)$ *is the steady-state solution.*

In Definition 1, there exists a unique periodic solution $\overline{x}_E(t)$ [42, Theorem 2.1.1 and Example 2.1.1]. If $A = 0$ holds, the solution is trivial, i.e., $\overline{x}_E(t) = 0$. The steady-state solutions satisfy the well-known superposition principle [43, Chapter 4] as shown below. The following proposition simply adapts the superposition principle to our formulations in this study.

Proposition 1 (Superposition Principle): For any $\omega_{in} > 0$, $A_\ell \in \mathbb{R}$, $\theta_\ell \in \mathbb{R}$, *and* $w_\ell \in \mathbb{R}$ $(\ell = 1, 2, \ldots, N_\ell)$, *if the waves are given by*

$$E_\ell(t) := A_\ell\cos(\omega_{in}t + \theta_\ell), \tag{10}$$

$$E_{sum}(t) := \sum_{\ell=1}^{N_\ell} w_\ell E_\ell(t), \tag{11}$$

the corresponding steady-state solutions satisfy

$$\overline{x}_{E_{sum}}(t) = \sum_{\ell=1}^{N_\ell} w_\ell \overline{x}_{E_\ell}(t). \tag{12}$$

Assuming that the reference wave $E_r(t)$ is given in the form of (10), using Proposition 1 decomposes the steady-state solutions $\overline{x}(t)$ included in the index $\overline{J}(E_r, f_c, \theta_{in}^+, \theta_{in}^-)$ as follows:

$$\begin{aligned}
&\overline{J}(E_r, f_c, \theta_{in}^+, \theta_{in}^-) \\
&= \left|\frac{I_1}{T_1}\int_0^{T_1} (\overline{x}^+(t) + \overline{x}^-(t))(\overline{x}^+(t) - \overline{x}^-(t))f_c(t)dt\right| \\
&= \left|\frac{I_1}{T_1}\int_0^{T_1} (\overline{x}_{E_{in}^+ - E_r}(t) + \overline{x}_{E_{in}^- - E_r}(t)) \right. \\
&\qquad \left. \times(\overline{x}_{E_{in}^+ - E_r}(t) - \overline{x}_{E_{in}^- - E_r}(t))f_c(t)dt\right| \\
&= \left|\frac{I_1}{T_1}\int_0^{T_1} (-2\overline{x}_{E_r}(t) + \overline{x}_{E_{in}^+ + E_{in}^-}(t))\overline{x}_{E_{in}^+ - E_{in}^-}(t)f_c(t)dt\right|.
\end{aligned} \tag{13}$$

The form derived above is tractable because the solution $\overline{x}_{E_r}(t)$ corresponding to the reference wave is separated from the others. This form enables the determination of a simple receiver structure, as described in the next subsection.

B. MAIN RESULTS: TWO TYPES OF SIMPLE STRUCTURES

Based on the performance index $\overline{J}(E_r, f_c, \theta_{in}^+, \theta_{in}^-)$ transformed in (13), we derive two types of simple structures for the receiver along with performance enhancement. Theorems 1 and 2 presented below are the main contributions of this study. First, Theorem 1 suggests the assumption $f_c(t) = 1$ implying that there is no carrier signal, as illustrated in Fig. 2 (a). Second, Theorem 2 assumes $E_r(t) = 0$, i.e., there is no reference wave, as shown in Fig. 2 (b). Let us define a coefficient for brief notation:

$$\tilde{A} := \frac{qA_{in}}{\sqrt{(k - m\omega_{in}^2)^2 + (\gamma\omega_{in})^2}}. \tag{14}$$

Theorem 1 (Receiver Without a Carrier Signal): Suppose that the following properties hold:

$$f_c(t) = 1, \tag{15}$$

$$E_r(t) = -\eta E_{in}^+(t) + (1 + \eta)E_{in}^-(t). \tag{16}$$

Then, the performance index $\overline{J}(E_r, f_c, \theta_{in}^+, \theta_{in}^-)$ *is given by*

$$\overline{J}(E_r, f_c, \theta_{in}^+, \theta_{in}^-) = |I_1\tilde{A}^2(2\eta + 1)|(1 - \cos(\theta_{in}^- - \theta_{in}^+)). \tag{17}$$

Furthermore, if the condition

$$\theta_{in}^- - \theta_{in}^+ = \pi, \tag{18}$$

holds, the performance index $\overline{J}(E_r, f_c, \theta_{in}^+, \theta_{in}^-)$ *is maximized with respect to* θ_{in}^+ *and* θ_{in}^-*:*

$$\max_{\theta_{in}^+, \theta_{in}^-} \overline{J}(E_r, f_c, \theta_{in}^+, \theta_{in}^-) = |I_1\tilde{A}^2(4\eta + 2)|. \tag{19}$$

Proof: The proof is given in Appendix. □

Theorem 2 (Receiver Without a Reference Wave): Suppose that the following properties hold for a given θ_c*:*

$$E_r(t) = 0, \tag{20}$$

$$f_c(t) = \sqrt{2}\sin(2\omega_{in}t + \theta_c), \tag{21}$$

$$\theta_{in}^+ = -\theta_{in}^-. \tag{22}$$

Then, the performance index $\overline{J}(E_r, f_c, \theta_{in}^+, \theta_{in}^-)$ *is given by*

$$\overline{J}(E_r, f_c, \theta_{in}^+, \theta_{in}^-) = \frac{|I_1\tilde{A}^2\sin(2\theta_{in}^-)\cos(\theta_c - 2\overline{\theta})|}{\sqrt{2}}, \tag{23}$$

where

$$\overline{\theta} := -\arctan\frac{\gamma\omega_{in}}{k - m\omega_{in}^2}. \tag{24}$$

Furthermore, if the conditions

$$\theta_{in}^- = -\theta_{in}^+ = \pi/4, \tag{25}$$

$$\theta_c = 2\overline{\theta}, \tag{26}$$

hold, the performance index $\overline{J}(E_r, f_c, \theta_{in}^+, \theta_{in}^-)$ *is maximized with respect to* θ_{in}^+, θ_{in}^-, *and* θ_c*:*

$$\max_{\theta_{in}^+, \theta_{in}^-, \theta_c} \overline{J}(E_r, f_c, \theta_{in}^+, \theta_{in}^-) = \frac{|I_1\tilde{A}^2|}{\sqrt{2}}. \tag{27}$$

Proof: The proof is given in Appendix. □

Designing the receiver based on Theorems 1 and 2 simplifies its structure, eliminating the need for a carrier signal or reference wave. Furthermore, the theorems provide the closed forms (17) and (23) of the approximated performance index $\overline{J}(E_r, f_c, \theta_{in}^+, \theta_{in}^-)$. By virtue of such forms, $\overline{J}(E_r, f_c, \theta_{in}^+, \theta_{in}^-)$ has been maximized with respect to the relevant parameters.

TABLE 1. Parameter setting for the simulation.

	Description	Value
V	External voltage	100 [V]
L	Length of the CNT	1.0×10^{-6} [m]
h_0	Gap between the anode and CNT	8.0×10^{-8} [m]
$A_{\rm in}$	Amplitude of the incoming wave	1.0×10^{4} [V/m]
$\omega_{\rm in}$	Angular frequency of the incoming wave	2π [rad] $\times 33.3$ [MHz]
m	Effective mass	8.541×10^{-21} [kg]
γ	Viscosity	5.218×10^{-13} [N·s/m]
k	Elasticity	3.905×10^{-4} [N/m]
q	Amount of charge around the tip	2.826×10^{-17} [C]
I_1	Coefficient for the field emission current	$-2.748 \times 10^{+11}$ [A/m^2]

TABLE 2. Settings for the two types of simplified receivers.

	Theorem 1 without a carrier signal	Theorem 2 without a reference wave
$E_{\rm r}(t)$	(16)	0
$f_{\rm c}(t)$	1	See (21) and (26)
η	0.5	Not used
$\theta_{\rm in}^{+}$	0	$-\pi/4$
$\theta_{\rm in}^{-}$	π	$\pi/4$

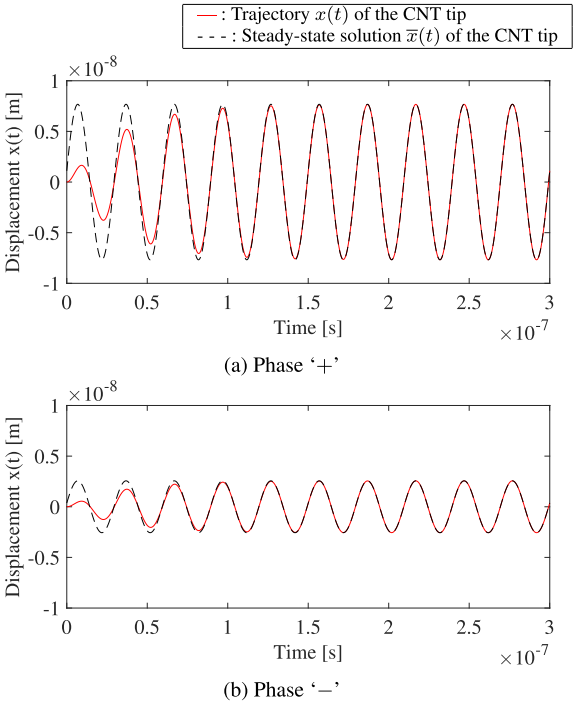

FIGURE 3. Vibrations of the CNT without a carrier signal. The solid and dashed lines represent the trajectories of the CNT tip $x(t)$ and its steady-state solution $\overline{x}(t)$, respectively.

V. NUMERICAL EVALUATION

The proposed design method is demonstrated through a numerical simulation. In Section V-A, the settings of the simulation and proposed method are described. In Section V-B, the receiver is evaluated without a carrier signal according to Theorem 1 and without a reference wave following Theorem 2, respectively.

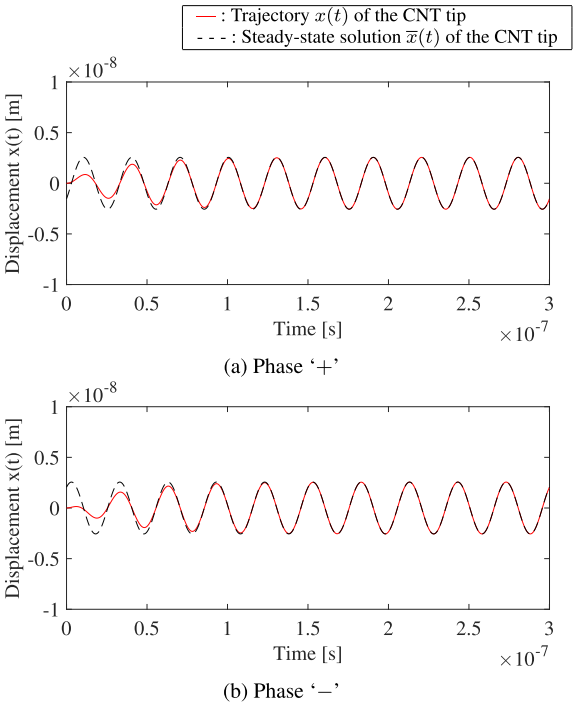

FIGURE 4. Vibrations of the CNT without a reference wave. The solid and dashed lines represent the trajectories of the CNT tip $x(t)$ and its steady-state solution $\overline{x}(t)$, respectively.

A. SETTINGS

Table 1 lists the receiver parameters used in the numerical simulation. The values of the external voltage V and the CNT length L are set according to the existing work [29]. The gap h_0 between the anode and CNT is set to a designed value that was previously used in a fabrication process [41]. The angular frequency $\omega_{\rm in}$ is set to the resonant angular frequency of the CNT such that it is well oscillated. The amplitude $A_{\rm in}$ of the incoming wave is set such that the assumption of a small displacement of the CNT tip is not violated. Note that the values of the CNT length L and gap h_0 are set based on our fabrication process [44], [45], which allows us to control these physical properties. The other parameters m, γ, k, q, and I_1 are set according to those of the existing work [41], which describes the detailed derivation of these settings. In the proposed method, the functions/parameters $E_{\rm r}(t)$, $f_{\rm c}(t)$, $\theta_{\rm in}^{+}$, $\theta_{\rm in}^{-}$, and η are designed using Theorems 1 and 2. The settings for the two types of receivers are listed in Table 2. Recall that $f_{\rm c}(t) = 1$ and $E_{\rm r}(t) = 0$ imply that no carrier signal and no reference wave are employed, respectively.

B. RESULTS

We first evaluated the simplified receiver motion in the numerical simulation. Figure 3 shows the vibrations of the CNT tip for both the phases '+' and '−' of the incoming wave without a carrier signal. It can be observed that the vibration amplitudes were different between both the phases of the incoming wave, whereas the vibration phases were equivalent. Figure 4 depicts the vibrations of the CNT tip without a reference wave. The vibration amplitudes were

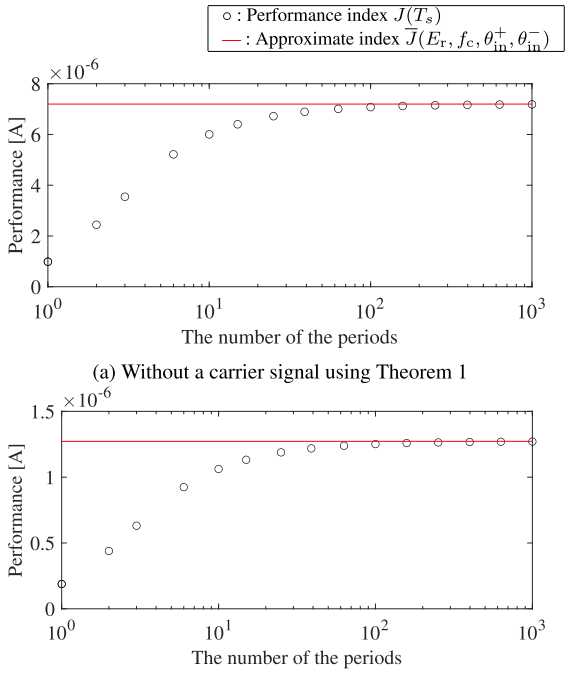

FIGURE 5. Performance index for the two types of receivers. The circles and line represent the index $J(T_s)$ and its approximation $\overline{J}(E_r, f_c, \theta_{in}^+, \theta_{in}^-)$, respectively.

equivalent between both the phases, but the vibration phases were different. These differences contribute to increasing the performance index $J(T_s)$.

Figure 5 displays the results of the performance index $J(T_s)$ with its approximation $\overline{J}(E_r, f_c, \theta_{in}^+, \theta_{in}^-)$ for the two types of structures. Because of the obtained results depicted in Figs. 3 and 4, positive values of $J(T_s)$ were excited, even if either the carrier signal or reference wave was not implemented. Furthermore, $J(T_s)$ became close to the approximation as the number of periods s increased. These results confirmed the effectiveness of the proposed design method using the theorems.

VI. CONCLUSION

We proposed a design method to simplify a nanoscale receiver structure and enhance the phase detection performance, in this study. The performance index denotes the difference between the output signals corresponding to the two phases. The proposed technique decomposes the approximated performance index into a tractable form. Analysis of this tractable form yields the mathematical conditions under which either the carrier signal or reference wave is excluded from the receiver, simplifying its structure. Moreover, the performance index is approximately maximized under these conditions. No carrier signal or no reference wave is then employed, enhancing the performance.

The proposed receiver omits either the reference wave or carrier signal, in contrast to the existing receiver [29]. This exclusion contributes the advantage of the receiver being infinitesimal because additional devices to generate such a wave and signal are not needed. Meanwhile, other components such as the CNT cantilever are equivalent between the proposed and existing receivers. No additional component is needed to realize the proposed simplification.

Future work will be aimed at implementing our CNT-based receivers in the real world. The relevant work [44] has fabricated and validated a CNT-based receiver, and it has a structure similar to the receiver focused on in this study. Moreover, the relevant work [46] has investigated the vacuum cavity fabrication of nano-electromechanical systems by using vapor etching. By virtue of this contribution, it is further expected that CNT-based receivers with a vacuum encapsulation will be established.

Our theoretically proposed method is based on the Duffing equation, which is often employed to describe nanomechanical resonators. In future work, we will improve the introduced concept by considering strain- and stress-driven nonlocal mechanics. We will also experimentally validate the introduced concept. We believe that this study can contribute to the development of nanoscale sensors with future potential.

APPENDIX
PROOF
A. PROOF OF THEOREM 1

Substituting $f_c(t) = 1$ and (16) into the performance index $\overline{J}(E_r, f_c, \theta_{in}^+, \theta_{in}^-)$ in (13) yields

$$\begin{aligned}
&\overline{J}(E_r, f_c, \theta_{in}^+, \theta_{in}^-) \\
&= \left| \frac{I_1}{T_1} \int_0^{T_1} (-2\overline{x}_{(-\eta E_{in}^+ + (\eta+1)E_{in}^-)}(t) + \overline{x}_{E_{in}^+ + E_{in}^-}(t)) \right. \\
&\qquad \left. \times \overline{x}_{E_{in}^+ - E_{in}^-}(t) \mathrm{d}t \right| \\
&= \left| \frac{I_1}{T_1} \int_0^{T_1} (2\eta+1) \overline{x}_{E_{in}^+ - E_{in}^-}(t)^2 \mathrm{d}t \right| \\
&= \frac{|I_1(2\eta+1)|}{T_1} \int_0^{T_1} \overline{x}_{E_{in}^+ - E_{in}^-}(t)^2 \mathrm{d}t. \qquad (28)
\end{aligned}$$

The relation

$$\begin{aligned}
&E_{in}^+(t) - E_{in}^-(t) \\
&\quad = A_{in} \cos(\omega_{in} t + \theta_{in}^+) - A_{in} \cos(\omega_{in} t + \theta_{in}^-) \\
&\quad = \sqrt{2 - 2\cos(\theta_{in}^- - \theta_{in}^+)} A_{in} \cos(\omega_{in} t + \theta_1), \qquad (29)
\end{aligned}$$

holds for some θ_1. Using this relation, for some θ_2, the steady-state solution $\overline{x}_{E_{in}^+ - E_{in}^-}(t)$ is described as follows:

$$\overline{x}_{E_{in}^+ - E_{in}^-}(t) = \sqrt{2 - 2\cos(\theta_{in}^- - \theta_{in}^+)} \tilde{A} \cos(\omega_{in} t + \theta_2). \qquad (30)$$

Because $\int_0^{T_1} \cos^2(\omega_{in} t + \theta_2) \mathrm{d}t = T_1/2$ holds for any θ_2, substituting (30) into (28) yields (17) as follows:

$$\begin{aligned}
&\overline{J}(E_r, f_c, \theta_{in}^+, \theta_{in}^-) \\
&\quad = \frac{|I_1(2\eta+1)|}{T_1} \left(\sqrt{2 - 2\cos(\theta_{in}^- - \theta_{in}^+)} \tilde{A} \right)^2 \frac{T_1}{2} \\
&\quad = |I_1(2\eta+1)|(1 - \cos(\theta_{in}^- - \theta_{in}^+)) \tilde{A}^2. \qquad (31)
\end{aligned}$$

Next, if (18) holds, $(1-\cos(\theta_{\rm in}^- - \theta_{\rm in}^+)) \le 2$ in (17) is maximized, leading to (19). This completes the proof. □

B. PROOF OF THEOREM 2

Because of the condition (22), the following relations hold:

$$\begin{aligned} E_{\rm in}^+(t) + E_{\rm in}^-(t) &= A_{\rm in}\cos(\omega_{\rm in}t - \theta_{\rm in}^-) + A_{\rm in}\cos(\omega_{\rm in}t + \theta_{\rm in}^-) \\ &= 2A_{\rm in}\cos(\omega_{\rm in}t)\cos(\theta_{\rm in}^-), \qquad (32) \\ E_{\rm in}^+(t) - E_{\rm in}^-(t) &= A_{\rm in}\cos(\omega_{\rm in}t - \theta_{\rm in}^-) - A_{\rm in}\cos(\omega_{\rm in}t + \theta_{\rm in}^-) \\ &= 2A_{\rm in}\sin(\omega_{\rm in}t)\sin(\theta_{\rm in}^-). \qquad (33) \end{aligned}$$

The steady-state solutions with respect to $E_{\rm in}^+(t) \pm E_{\rm in}^-(t)$ are given as

$$\bar{x}_{E_{\rm in}^+ + E_{\rm in}^-}(t) = 2\tilde{A}\cos(\theta_{\rm in}^-)\cos(\omega_{\rm in}t + \bar{\theta}'), \qquad (34)$$

$$\bar{x}_{E_{\rm in}^+ - E_{\rm in}^-}(t) = 2\tilde{A}\sin(\theta_{\rm in}^-)\sin(\omega_{\rm in}t + \bar{\theta}'), \qquad (35)$$

where $\bar{\theta}' \in \{\bar{\theta}, \bar{\theta} - \pi\}$. Substituting $E_{\rm r}(t) = 0$, (34), and (35) into (13) yields

$$\begin{aligned} &\bar{J}(E_{\rm r}, f_{\rm c}, \theta_{\rm in}^+, \theta_{\rm in}^-) \\ &= \left| \frac{I_1}{T_1}\int_0^{T_1} \bar{x}_{E_{\rm in}^+ + E_{\rm in}^-}(t)\bar{x}_{E_{\rm in}^+ - E_{\rm in}^-}(t) f_{\rm c}(t)\mathrm{d}t \right| \\ &= \left| \frac{I_1\tilde{A}^2}{T_1}\int_0^{T_1} 4\cos(\theta_{\rm in}^-)\sin(\theta_{\rm in}^-)\cos(\omega_{\rm in}t + \bar{\theta}') \right. \\ &\qquad \left. \times \sin(\omega_{\rm in}t + \bar{\theta}') f_{\rm c}(t)\mathrm{d}t \right| \\ &= \left| \frac{I_1\tilde{A}^2\sin(2\theta_{\rm in}^-)}{T_1}\int_0^{T_1} \sin(2\omega_{\rm in}t + 2\bar{\theta}') f_{\rm c}(t)\mathrm{d}t \right| \\ &= \left| \frac{I_1\tilde{A}^2\sin(2\theta_{\rm in}^-)}{T_1}\int_0^{T_1} \sin(2\omega_{\rm in}t + 2\bar{\theta}) f_{\rm c}(t)\mathrm{d}t \right|. \qquad (36) \end{aligned}$$

Meanwhile, the carrier signal $f_{\rm c}(t)$ is expressed as

$$\begin{aligned} f_{\rm c}(t) &= \sqrt{2}\sin(2\omega_{\rm in}t + 2\bar{\theta} + (\theta_{\rm c} - 2\bar{\theta})) \\ &= \sqrt{2}\sin(2\omega_{\rm in}t + 2\bar{\theta})\cos(\theta_{\rm c} - 2\bar{\theta}) \\ &\quad + \sqrt{2}\cos(2\omega_{\rm in}t + 2\bar{\theta})\sin(\theta_{\rm c} - 2\bar{\theta}). \qquad (37) \end{aligned}$$

Because of the orthogonal properties, we obtain

$$\int_0^{T_1} \sin^2(2\omega_{\rm in}t + 2\bar{\theta})\mathrm{d}t = \frac{T_1}{2}, \qquad (38)$$

$$\int_0^{T_1} \sin(2\omega_{\rm in}t + 2\bar{\theta})\cos(2\omega_{\rm in}t + 2\bar{\theta})\mathrm{d}t = 0. \qquad (39)$$

Using these properties, substituting (37) into (36) yields (23):

$$\begin{aligned} &\bar{J}(E_{\rm r}, f_{\rm c}, \theta_{\rm in}^+, \theta_{\rm in}^-) \\ &= \left| \frac{I_1\tilde{A}^2\sin(2\theta_{\rm in}^-)}{T_1} \right. \\ &\qquad \left. \times \int_0^{T_1} \sqrt{2}\cos(\theta_{\rm c} - 2\bar{\theta})\sin^2(2\omega_{\rm in}t + 2\bar{\theta})\mathrm{d}t \right| \\ &= \left| \frac{I_1\tilde{A}^2\sin(2\theta_{\rm in}^-)}{T_1}\sqrt{2}\cos(\theta_{\rm c} - 2\bar{\theta})\frac{T_1}{2} \right| \\ &= \frac{|I_1\tilde{A}^2\sin(2\theta_{\rm in}^-)\cos(\theta_{\rm c} - 2\bar{\theta})|}{\sqrt{2}}. \qquad (40) \end{aligned}$$

The statement (27) clearly holds because $\sin(2\theta_{\rm in}^-)\cos(\theta_{\rm c} - 2\bar{\theta}) \le 1$ holds in (23). This completes the proof. □

ACKNOWLEDGMENT

The authors would like to thank Editage (www.editage.jp) for English language editing.

REFERENCES

[1] M. Dykman, *Fluctuating Nonlinear Oscillators: From Nanomechanics to Quantum Superconducting Circuits*. Oxford, U.K.: Oxford Univ. Press, 2012, doi: 10.1093/acprof:oso/9780199691388.001.0001.

[2] S. Schmid, L. G. Villanueva, and M. L. Roukes, *Fundamentals Nanomechanical Resonators*. Cham, Switzerland: Springer, 2016, doi: 10.1007/978-3-319-28691-4.

[3] K. Eom, H. S. Park, D. S. Yoon, and T. Kwon, "Nanomechanical resonators and their applications in biological/chemical detection: Nanomechanics principles," *Phys. Rep.*, vol. 503, pp. 115–163, Jun. 2011, doi: 10.1016/j.physrep.2011.03.002.

[4] B. Arash, J.-W. Jiang, and T. Rabczuk, "A review on nanomechanical resonators and their applications in sensors and molecular transportation," *Appl. Phys. Rev.*, vol. 2, no. 2, Jun. 2015, Art. no. 021301, doi: 10.1063/1.4916728.

[5] P. M. Kosaka, V. Pini, J. J. Ruz, R. A. da Silva, M. U. González, D. Ramos, M. Calleja, and J. Tamayo, "Detection of cancer biomarkers in serum using a hybrid mechanical and optoplasmonic nanosensor," *Nature Nanotechnol.*, vol. 9, no. 12, pp. 1047–1053, Dec. 2014, doi: 10.1038/nnano.2014.250.

[6] K. Jensen, K. Kim, and A. Zettl, "An atomic-resolution nanomechanical mass sensor," *Nature Nanotechnol.*, vol. 3, no. 9, pp. 533–537, Sep. 2008, doi: 10.1038/nnano.2008.200.

[7] J. Moser, J. Güttinger, A. Eichler, and M. J. Esplandiu, "Ultrasensitive force detection with a nanotube mechanical resonator," *Nature Nanotechnol.*, vol. 8, pp. 493–496, Jun. 2013, doi: 10.1038/nnano.2013.97.

[8] J. Chaste, A. Eichler, J. Moser, G. Ceballos, R. Rurali, and A. Bachtold, "A nanomechanical mass sensor with yoctogram resolution," *Nature Nanotechnol.*, vol. 7, no. 5, pp. 301–304, 2012, doi: 10.1038/nnano.2012.42.

[9] V. C. Meesala, M. R. Hajj, and E. Abdel-Rahman, "Bifurcation-based MEMS mass sensors," *Int. J. Mech. Sci.*, vol. 180, Aug. 2020, Art. no. 105705, doi: 10.1016/j.ijmecsci.2020.105705.

[10] I. F. Akyildiz and J. M. Jornet, "Electromagnetic wireless nanosensor networks," *Nano Commun. Netw.*, vol. 1, no. 1, pp. 3–19, Mar. 2010, doi: 10.1016/j.nancom.2010.04.001.

[11] I. F. Akyildiz and J. M. Jornet, "The Internet of Nano-Things," *IEEE Wireless Commun.*, vol. 17, no. 6, pp. 58–63, Dec. 2010, doi: 10.1109/MWC.2010.5675779.

[12] S. Balasubramaniam and J. Kangasharju, "Realizing the Internet of Nano Things: Challenges, solutions, and applications," *Computer*, vol. 46, no. 2, pp. 62–68, 2013, doi: 10.1109/MC.2012.389.

[13] A. O. Balghusoon and S. Mahfoudh, "Routing protocols for wireless nanosensor networks and Internet of Nano Things: A comprehensive survey," *IEEE Access*, vol. 8, pp. 200724–200748, 2020, doi: 10.1109/ACCESS.2020.3035646.

[14] N. Abuali, S. Aleyadeh, F. Djebbar, A. Alomainy, M. M. Ali Almaazmi, and S. Al Ghaithi, "Performance evaluation of routing protocols in electromagnetic nanonetworks," *IEEE Access*, vol. 6, pp. 35908–35914, 2018, doi: 10.1109/ACCESS.2018.2845305.

[15] S. Canovas-Carrasco, R. M. Sandoval, A.-J. Garcia-Sanchez, and J. Garcia-Haro, "Optimal transmission policy derivation for IoNT flow-guided nanosensor networks," *IEEE Internet Things J.*, vol. 6, no. 2, pp. 2288–2298, Apr. 2019, doi: 10.1109/jiot.2019.2906015.

[16] L. Zhou, G. Han, and L. Liu, "Pulse-based distance accumulation localization algorithm for wireless nanosensor networks," *IEEE Access*, vol. 5, pp. 14380–14390, 2017, doi: 10.1109/ACCESS.2017.2732351.

[17] P. K. D. Pramanik, A. Solanki, A. Debnath, A. Nayyar, S. El-Sappagh, and K. Kwak, "Advancing modern healthcare with nanotechnology, nanobiosensors, and Internet of Nano Things: Taxonomies, applications, architecture, and challenges," *IEEE Access*, vol. 8, pp. 65230–65266, 2020, doi: 10.1109/ACCESS.2020.2984269.

[18] Q. Abbasi, K. Yang, N. Chopra, and J. M. Jornet, "Nano-communication for biomedical applications: A review on the state-of-the-art from physical layers to novel networking concepts," *IEEE Access*, vol. 4, pp. 3920–3935, 2016, doi: 10.1109/ACCESS.2016.2593582.
[19] F. Afsana, M. Asif-Ur-Rahman, M. R. Ahmed, M. Mahmud, and M. S. Kaiser, "An energy conserving routing scheme for wireless body sensor nanonetwork communication," *IEEE Access*, vol. 6, pp. 9186–9200, 2018, doi: 10.1109/ACCESS.2018.2789437.
[20] S. Nishibori, T. Murase, and Y. Tadokoro, "Periodic networked imaging with nanoscale sensor nodes via two-layered time-division access," *IEEE Internet Things J.*, early access, Sep. 21, 2021, doi: 10.1109/jiot.2021.3112711.
[21] T. Nobunaga, H. Tanaka, and Y. Tadokoro, "Reconstruction for spatially distributed single-pixel imaging based on pattern filtering," *IEEE Signal Process. Lett.*, vol. 25, no. 5, pp. 705–709, May 2018, doi: 10.1109/lsp.2018.2816579.
[22] A. Rizwan, A. Zoha, R. Zhang, W. Ahmad, K. Arshad, N. A. Ali, A. Alomainy, M. A. Imran, and Q. H. Abbasi, "A review on the role of nano-communication in future healthcare systems: A big data analytics perspective," *IEEE Access*, vol. 6, pp. 41903–41920, 2018, doi: 10.1109/ACCESS.2018.2859340.
[23] W. L. Stutzman and G. A. Thiele, *Antenna Theory Design*. New York, NY, USA: Wiley, 1981.
[24] J. M. Jornet and I. F. Akyildiz, "Joint energy harvesting and communication analysis for perpetual wireless nanosensor networks in the terahertz band," *IEEE Trans. Nanotechnol.*, vol. 11, no. 3, pp. 570–580, May 2012, doi: 10.1109/TNANO.2012.2186313.
[25] J. M. Jornet and I. F. Akyildiz, "Graphene-based plasmonic nano-antenna for terahertz band communication in nanonetworks," *IEEE J. Sel. Areas Commun.*, vol. 31, no. 12, pp. 685–694, Dec. 2013, doi: 10.1109/JSAC.2013.SUP2.1213001.
[26] S. Sugiura and H. Iizuka, "Deep-subwavelength MIMO using graphene-based nanoscale communication channel," *IEEE Access*, vol. 2, pp. 1240–1247, 2014, doi: 10.1109/ACCESS.2014.2364091.
[27] K. Jensen, J. Weldon, H. Garcia, and A. Zettl, "Nanotube radio," *Nano Lett.*, vol. 7, no. 11, pp. 3508–3511, 2007, doi: 10.1021/nl0721113.
[28] P. Vincent, P. Poncharal, T. Barois, S. Perisanu, V. Gouttenoire, H. Frachon, A. Lazarus, E. de Langre, E. Minoux, M. Charles, A. Ziaei, D. Guillot, M. Choueib, A. Ayari, and S. T. Purcell, "Performance of field-emitting resonating carbon nanotubes as radio-frequency demodulators," *Phys. Rev. B, Condens. Matter*, vol. 83, Dec. 2011, Art. no. 155446, doi: 10.1103/PhysRevB.83.155446.
[29] Y. Tadokoro, Y. Ohno, and H. Tanaka, "Detection of digitally phase-modulated signals utilizing mechanical vibration of CNT cantilever," *IEEE Trans. Nanotechnol.*, vol. 17, no. 1, pp. 84–92, Jan. 2018, doi: 10.1109/TNANO.2017.2765310.
[30] A. E. Hassanien, M. Breen, M.-H. Li, and S. Gong, "Acoustically driven electromagnetic radiating elements," *Sci. Rep.*, vol. 10, no. 1, Dec. 2020, Art. no. 17006, doi: 10.1038/s41598-020-73973-6.
[31] J. A. Boales, F. Mateen, and P. Mohanty, "Optical wireless information transfer with nonlinear micromechanical resonators," *Microsyst. Nanoeng.*, vol. 3, no. 1, p. 17026, Dec. 2017, doi: 10.1038/micronano.2017.26.
[32] H. Chen, X. Liang, C. Dong, Y. He, N. Sun, M. Zaeimbashi, Y. He, Y. Gao, P. V. Parimi, H. Lin, and N.-X. Sun, "Ultra-compact mechanical antennas," *Appl. Phys. Lett.*, vol. 117, no. 17, 2020, Art. no. 170501, doi: 10.1063/5.0025362.
[33] A. Ayari, P. Vincent, S. Perisanu, M. Choueib, V. Gouttenoire, M. Bechelany, D. Cornu, and S. T. Purcell, "Self-oscillations in field emission nanowire mechanical resonators: A nanometric DC-AC conversion," *Nano Lett.*, vol. 7, no. 8, pp. 2252–2257, Aug. 2007, doi: 10.1021/nl070742r.
[34] J. Moser, A. Eichler, J. Güttinger, M. I. Dykman, and A. Bachtold, "Nanotube mechanical resonators with quality factors of up to 5 million," *Nature Nanotechnol.*, vol. 9, no. 12, pp. 1007–1011, Dec. 2014, doi: 10.1038/nnano.2014.234.
[35] J. S. Aldridge and A. N. Cleland, "Noise-enabled precision measurements of a duffing nanomechanical resonator," *Phys. Rev. Lett.*, vol. 94, no. 15, Apr. 2005, Art. no. 156403, doi: 10.1103/physrevlett.94.156403.
[36] G. A. Steele, A. K. Hättel, B. Witkamp, M. Poot, H. B. Meerwaldt, L. P. Kouwenhoven, and H. S. J. van der Zant, "Strong coupling between single-electron tunneling and nanomechanical motion," *Science*, vol. 325, no. 5944, pp. 1103–1107, Aug. 2009, doi: 10.1126/science.1176076.
[37] M. A. Eltaher, M. E. Khater, and S. A. Emam, "A review on nonlocal elastic models for bending, buckling, vibrations, and wave propagation of nanoscale beams," *Appl. Math. Model.*, vol. 40, nos. 5–6, pp. 4109–4128, Mar. 2016, doi: 10.1016/j.apm.2015.11.026.
[38] G. Romano and R. Barretta, "Stress-driven versus strain-driven nonlocal integral model for elastic nano-beams," *Compos. B, Eng.*, vol. 114, pp. 184–188, Apr. 2017, doi: 10.1016/j.compositesb.2017.01.008.
[39] L. Behera and S. Chakraverty, "Recent researches on nonlocal elasticity theory in the vibration of carbon nanotubes using beam models: A review," *Arch. Comput. Methods Eng.*, vol. 24, no. 3, pp. 481–494, Jul. 2017, doi: 10.1007/s11831-016-9179-y.
[40] Y. Tadokoro, H. Tanaka, and M. I. Dykman, "Driven nonlinear nanomechanical resonators as digital signal detectors," *Sci. Rep.*, vol. 8, May 2018, Art. no. 11284, doi: 10.1038/s41598-018-29572-7.
[41] Y. Ito, K. Funayama, J. Hirotani, Y. Ohno, and Y. Tadokoro, "Stochastic optimal control to minimize the impact of manufacturing variations on nanomechanical systems," *IEEE Access*, vol. 7, pp. 171195–171205, 2019, doi: 10.1109/ACCESS.2019.2955697.
[42] M. Farkas, *Periodic Motions*. New York, NY, USA: Springer-Verlag, 1994.
[43] A. Bacciotti, *Stability Control Linear System*. Cham, Switzerland: Springer, 2019, doi: 10.1007/978-3-030-02405-5.
[44] K. Funayama, H. Tanaka, J. Hirotani, K. Shimaoka, Y. Ohno, and Y. Tadokoro, "Carbon nanotube-based nanomechanical receiver for digital data transfer," *ACS Appl. Nano Mater.*, Oct. 2021, doi: 10.1021/acsanm.1c02563.
[45] K. Funayama, H. Tanaka, J. Hirotani, K. Shimaoka, Y. Ohno, and Y. Tadokoro, "Dynamic range enhancement via linearized output in nanoelectromechanical systems by combining high-order harmonics," *IEEE Trans. Circuits Syst. II, Exp. Briefs*, vol. 68, no. 10, pp. 3251–3255, Oct. 2021, doi: 10.1109/tcsii.2021.3062390.
[46] A. Miura, K. Shimaoka, K. Funayama, H. Tanaka, and Y. Tadokoro, "A consideration of semipermeable membrane structure for vacuum cavity fabrication using vapor etching," *IEEJ Trans. Sensors Micromachines*, vol. 141, no. 10, pp. 364–365, Oct. 2021, doi: 10.1541/ieejsmas.141.364.

YUJI ITO (Member, IEEE) received the B.S., M.S., and Ph.D. degrees from Nagoya University, Aichi, Japan, in 2009, 2011, and 2014, respectively. Since 2011, he has been with Toyota Central Research and Development Labs., Inc., Japan. His research interests include stochastic systems theory and nonlinear optimal control. He is a member of the Society of Instrument and Control Engineers.

YUKIHIRO TADOKORO (Senior Member, IEEE) received the B.E., M.E., and Ph.D. degrees in information electronics engineering from Nagoya University, Aichi, Japan, in 2000, 2002, and 2005, respectively. Since 2006, he has been with Toyota Central Research and Development Labs., Inc., Japan. He was a Research Scholar with the Department of Physics and Astronomy, Michigan State University, East Lansing, MI, USA, in 2011 and 2012, to study nonlinear phenomena for future applications in signal and information processing fields. In 2019 and 2020, he was a Visiting Professor with the Graduate School of Informatics, Nagoya University. Since 2021, he has been an Executive Engineer at the Toyota Research Institute of North America, Ann Arbor, MI, USA. His current research interests include nanoscale wireless communication, quantum sensing systems, noise-related phenomena in nonlinear systems, and their applications in vehicles and smart city. He is a Senior Member of the Institute of Electronics, Information and Communication Engineers, Japan.